Ultrahigh Permittivity, Ultralow Loss and Stability in $(In_{0.5}Ta_{0.5})_{0.1}Ti_{0.9}O_2$ Ceramics With Temperature Range From -100 to 235 °C

Ying Xue
Shaanxi University of Science and Technology Xi'an Campus: Shaanxi University of Science and Technology

Zhuo Wang (wangzhuo@sust.edu.cn)
Shaanxi University of Science & Technology

Yanxin Li
Shaanxi University of Science and Technology Xi'an Campus: Shaanxi University of Science and Technology

Zhihui Yi
Shaanxi University of Science and Technology Xi'an Campus: Shaanxi University of Science and Technology

Xin Li
Shaanxi University of Science and Technology Xi'an Campus: Shaanxi University of Science and Technology

Dan Wu
Shaanxi University of Science and Technology Xi'an Campus: Shaanxi University of Science and Technology

Rapid Communication

Keywords: ultrahigh permittivity, ultralow dielectric loss, temperature stability

Posted Date: December 29th, 2021

DOI: https://doi.org/10.21203/rs.3.rs-1195430/v1

Abstract

Dielectric materials with excellent dielectric properties are being promoted in requirements of microelectronic devices. In this study, $(In_{0.5}Ta_{0.5})_{0.1}Ti_{0.9}O_2$ ceramics were achieved by a solid-state reaction with reducing atmosphere of N_2. Also, dense microstructure, ultrahigh permittivity (ε_r = 1.18 × 10^5) and ultralow dielectric loss (tanδ = 0.0072) were demonstrated at1 kHz. Interestingly enough, the temperature coefficient of permittivity which satisfies X9D (-100 °C - 235 °C, $\Delta\varepsilon_r/\varepsilon_{25°C}$ < ± 3.3 %) maintained stability at 1 kHz, and the dielectric mechanism could be connected to the electron-pinned defect dipoles (EPDD), which has favourable potential applications in electronic devices.

1. Introduction

As electronic devices continue to develop towards integration, intelligence and high performance, the development of dielectric materials has become a hot topic, especially the excellent high temperature range above 200°C at the engine compartment of new energy vehicles. Regrettably, it is difficult to develop applicable properties of dielectric materials for such applications. Understanding historical research, plenty of colossal permittivity (CP) materials were synthesized, including the $BaTiO_3$ ceramics and $ACu_3Ti_4O_{12}$ (*A* = Ca, Sr, Bi, Na, Cd) materials [1–4]. Although $BaTiO_3$ has been reported with excellent dielectric properties, the permittivity of pure $BaTiO_3$ near Tc which was 120°C fluctuates massively. Recently, a stable dielectric properties at temperature range for X7R (-55 - 125°C, $\Delta\varepsilon_r/\varepsilon_{25°C} \leq \pm 15\%$) applications were obtained in La^{3+} and Ca^{2+} ions co-doped $BaTiO_3$ samples with dielectric loss (tanδ = 0.04) and permittivity (ε_r = 2000) by Lu et al [5]. Also, Nb^{5+} and Ni^{2+} ions co-doped $BaTiO_3$ ceramics were investigated for X7R ceramics by Li et al [6]. Li et al. found the $BaTiO_3$-0.01Nb_2O_5-*x*MgO ceramics with permittivity (ε_r = 4.5 × 10^4), which merely satisfies the X8R (-55 - 150°C, $\Delta\varepsilon_r/\varepsilon_{25°C} \leq \pm 15\%$) requirement [7]. On the other hand, Wang et al. reported TiO_2 modified $CaCu_3Ti_4O_{12}$ ceramics which showed permittivity (ε_r = 6.81 × 10^4), but over 0.12 dielectric loss at 1 kHz [8]. Peng et al. reported dielectric loss (tanδ = 0.035) of $CdCu_3Ti_4O_{12}$ ceramics were reported through a sol-gel technique, only for X8R ceramics [9]. The results of the survey show high permittivity, low dielectric loss and excellent temperature stability cannot be achieved at the same time.

It is worth noting that $(In_{0.5}Nb_{0.5})_xTi_{1-x}O_2$ ceramics were prepared by Liu et al. using a solid-state method in 2013 [10], and the systems exhibited CP ($\varepsilon_r > 2 \times 10^4$) and low dielectric loss (tanδ < 0.05), simultaneously showed good frequency and temperature stability over wide ranges. Li et al. reported the $(La_{0.5}Nb_{0.5})_xTi_{1-x}O_2$ samples with dielectric loss (tanδ = 0.02896) and permittivity (ε_r = 49692), but the samples only fulfilled temperature stability for X8R [11]. Peng et al. prepared $(Ag_{1/4}Nb_{3/4})_{0.005}Ti_{0.995}O_2$ ceramics, obtained X9R (-55 - 200°C, $\Delta\varepsilon_r/\varepsilon_{25°C} \leq \pm 15\%$) requirements, but low permittivity and relatively high dielectric loss are 9410 and 0.037, respectively [12]. In 2017, the $(In_{0.5}Ta_{0.5})_xTi_{1-x}O_2$ ceramics were discussed by Hu et al., and the result of the system exhibited excellent dielectric properties with temperature stability from -223 - 127°C for *x* = 0.005 [13]. Plenty of researches paid attention to the

capacitance, loss parameters and others of TiO_2-based ceramics [14–21], but these reported materials which were difficult to balance permittivity, dielectric loss and temperature stability, especially further satisfy the requirements for high temperature industrial application above 150°C.

Compared with Nb^{5+} ion, Ta^{5+} ion has more one electron shell with the larger distortion resulting in stronger localization of the electron [13], which could result to the lower dielectric loss and more stable permittivity at a wide temperature range. On the other hand, ultrahigh permittivity needs more defect dipole clusters, so the higher permittivity could be obtained in ceramics by sintering in N_2 reducing atmosphere. In this work, the In^{3+} and Ta^{5+} co-doped TiO_2 ceramics based on the solid-state reaction method were synthesized in N_2 reducing atmosphere. The excellent dielectric properties with ultrahigh permittivity (1.18×10^5 at 1 kHz), ultralow dielectric loss (0.0072 at 1 kHz) and temperature stability which satisfies X9D (-100°C - 235°C, $\Delta\varepsilon_r/\varepsilon_{25°C} < \pm 3.3\%$) were exhibited.

2. Experimental Details

The $(In_{0.5}Ta_{0.5})_{0.1}Ti_{0.9}O_2$ (abbreviated by ITTO) ceramics were synthesized using a solid-state reaction process. The prepared materials of TiO_2 (99.99%, rutile, Aladdin), In_2O_3 (99.99%, Aladdin), and Ta_2O_5 (99.99%, Sinopharm) were dried for 24 h in a drying oven at 80°C. Next, these oxides were weighed with stoichiometric compositions and ball-milled in deionized water with zirconia balls for 6 hours. After pulverizing and drying, the powder was calcined at 1150°C in air for 2 hours. What's more, the preprocessed powder was made into pellets using a cold isostatic press. Finally, the samples were sintered at 1450°C for 4 h with N_2 reducing atmosphere.

The phase structure was executed using Raman spectroscopy (Renishaw-invia) and X-ray diffraction (XRD) technique (D8 advance, Germany), and the Rietveld refinement result was fitted using the GSAS software for the ITTO samples. The microstructure of hot-corrosion surface sample was achieved using scanning electron microscopy (SEM) (Regulus 8100, Hitachi). The precision impedance analyzer (Agilent-E4980A) was selected to determine dielectric properties of the ITTO ceramics. The X-ray photoelectron spectroscopy (XPS) (AXIS SUPRA Britain) was used to measure the valence states of the elements which was fitted using the Casa XPS software.

3. Results And Discussion

Figure 1(a) exhibited the Raman spectroscopy of ITTO samples, verifying the phase structure of the ceramic. Four characteristic peaks were observed, including B_{1g}, E_g, A_{1g} and the second-order effect in multi-phonon peak at 234 cm^{-1}. As a result, the Raman peak which verify the existence of the rutile TiO_2 crystal structure [16]. In terms of the Rietveld refinement, no distinct other phases were observed in ITTO samples in Figure 1(b). The lattice parameters (a = b = 4.614 Å and c = 2.980 Å) of the ITTO ceramics were achieved by Rietveld refinement are larger than (a = b = 4.593, c = 2.959 (JCPDS 21-1276)) for pure rutile TiO_2 [22]. As a result, the lattice size of the increase could be related to the Ta^{5+} and In^{3+} of larger

ionic radii instead of the Ti^{4+} ions, indicating Ta^{5+} and In^{3+} form a complete solid solution in rutile TiO_2 structure. Figure 1(c) exhibited the microstructure of hot-corrosion surface for the ITTO ceramics in detail, and dense sample, apparent grain and grain boundary were observed, no obvious impurity segregation and porosity, and Figure 1(d) exhibited the grain size almost 11.35 μm.

To reveal the dielectric properties in ITTO ceramics, Fig. 2(a) exhibited the frequency dependence of the dielectric loss and permittivity of the ITTO ceramics, which are 0.0072 and 1.18×10^5 at 1 kHz, respectively, including the good frequency and temperature stability. Meanwhile, Fig. 2(b) exhibited the temperature function of ITTO ceramics. The temperature coefficient of the sample is calculated between ± 3.3% at 1 kHz, which satisfies X9D (-100°C - 235°C, $\Delta\varepsilon_r/\varepsilon_{25°C} < \pm 3.3\%$), and Fig. 2(c) exhibited between ± 4.7% at 10 kHz, which satisfies X9E (-60°C - 300°C, $\Delta\varepsilon_r/\varepsilon_{25°C} < \pm 4.7\%$) requirements, far below the practical applications requirements. As shown in Fig. 2(d), the typical CP materials have been contrasted in detail. As a result, the ultralow dielectric loss, ultrahigh permittivity with temperature stability were obtained in ITTO ceramics. [5–9, 11, 23, 24]

To elucidate the influences of Ta^{5+} and In^{3+} co-doped TiO_2 structure in the sample on the potential dielectric mechanism. In Fig. 3, the XPS spectra of the ITTO ceramics were used to analyze the origin of CP, and different elements In, Ta, Ti, O were identified to the binding energies in the sample. Fig. 3(a) exhibited the binding energies (230.02 eV, 241.59 eV) of two peaks which confirmed the existence of Ta^{5+} [25]. Meanwhile, the binding energies (444.51 eV, 452.07 eV) of two peaks were assigned with the presence of In^{3+} in Fig. 3(b) [26].

$$In_2O_3 \xrightarrow{2TiO_2} 2In'_{Ti} + V_O^{\bullet\bullet} + 3O_O \quad (1)$$

Figure 3(c) exhibited the three energy peaks components of O1s profile, which can be confirmed as the bulk Ti-O bond (530.12 eV), oxygen vacancies (531.5 eV), and the surface hydroxyl (OH) (532.52 eV), respectively [27]. Another for Ti2p, two different peaks (458.79 eV, 464.63 eV) could be found in Figure 3(d), which can be suggested to the Ti^{4+} ion. Moreover, two small peaks indicate the existence of Ti^{3+} with lower binding energy of 459.5 eV and 463.86 eV [28]. Based on the pure rutile TiO_2, the adulteration of In^{3+} ion can form oxygen vacancies for charge compensation. While the Ta element instead of the Ti element, some extra electrons are generated, transforming Ti^{4+} ions to Ti^{3+} ions, as follows:

$$2TiO_2 + Ta_2O_5 \xrightarrow{4TiO_2} 2Ti'_{Ti} + 2Ta^{\bullet}_{Ti} + 8O_O + \frac{1}{2}O_2\uparrow \quad (2)$$

$Ti4^+ + e \rightarrow Ti^{3+}$ (3)

The $V_O^{\bullet\bullet}$ is the oxygen vacancy, the $Ta^{\bullet}_{Ti}$ represents Ta on the Ti lattice site, and the $In^{'}_{Ti}$ represents in on the Ti lattice site.

As discussed above, doping Ta^{5+} ions which create extra free electrons have a positive effect on transforming Ti^{4+} ions to Ti^{3+} ions, especially sintering in the N_2 reducing atmosphere, the result of ultrahigh permittivity is obtained. Combining with In^{3+} ions, which are introduced to facilitate oxygen vacancies forming, keeping an electric neutrality of the system and forming different complex cluster-defects, including $\mathrm{In}_2^{3+}\mathrm{V}_{\mathrm{O}}^{\bullet\bullet}\mathrm{Ti}^{3+}$, $\mathrm{Ta}_2^{5+}\mathrm{Ti}^{3+}A_{\mathrm{Ti}}(A = \mathrm{In}^{3+}, \mathrm{Ti}^{4+}, \mathrm{Ti}^{3+})$ and so on. The moving of electrons is limited because of the various defect dipole clusters, further obtaining ultralow dielectric loss, the result is consistent with Fig. 2(a). Further in high temperature ranges, the result of ultrahigh permittivity could be related to the defect clusters are polarized. Although most of the defect clusters could not be activated at the lower temperature ranges, the localizable electrons could be polarized as well as move in a short distance, achieving an ultrahigh permittivity. As a result, the excellent dielectric properties and temperature stability should be closely connected to the localization of various complex cluster-defects, which could be originated from the EPDD.

4. Conclusions

In summary, the ITTO ceramics with dense microstructure and exceptional dielectric properties were achieved by a solid-state reaction process with N_2 reducing atmosphere. At 1 kHz, it is worth promoting the ultrahigh permittivity ($\varepsilon_r = 1.18\times10^5$) and ultralow dielectric loss ($\tan\delta = 0.0072$) in microelectronic devices. Emphatically, the temperature coefficient of the sample is calculated at 1 kHz, which has potential applications in X9D (-100°C - 235°C, $\Delta\varepsilon_r/\varepsilon_{25°C} < \pm 3\%$) capacitor, and the excellent dielectric performances could be attributed to the EPDD. As an applicability, the excellent high temperature range above 200°C has potential requirement for the engine compartment of new energy vehicles.

Declarations

Acknowledgements

The present work was supported by the National Natural Science Foundation of China (51572160), the National Key Research and Development Program of Shaanxi Province (Grant 2021GY-224), and Graduate Innovation Fund of Shaanxi University of Science and Technology.

References

1. Lu D, Gao X, Liu Q. Synergistic effect of terbium and calcium ions on the temperature stability and dielectric loss of $BaTiO_3$-based ceramics. J Alloys Compd. 2019;808:151713.
2. Huang Z, Xue J, Ge Y, Qin J, Hou Y, Chu J, Zhang D. Temperature dependence of $BaTiO_3$ infrared dielectric properties. Appl Phys Lett. 2006;88:212902.
3. Peng Z, Liang P, Wang X, Peng H, Chen X, Yang Z, Chao X. Fabrication and characterization of $CdCu_3Ti_4O_{12}$ ceramics with colossal permittivity and low dielectric loss. Mater Lett. 2018;210:301–4.

4. Boonlakhorn J, Kidkhunthod P, Chanlek N, Thongbai P. (Al^{3+}, Nb^{5+}) co-doped $CaCu_3Ti_4O_{12}$: an extended approach for acceptor-donor heteroatomic substitutions to achieve high-performance giant-dielectric permittivity. J Eur Ceram Soc. 2018;38:137–43.
5. Lu D, Yue Y, Sun X. Novel X7R $BaTiO_3$ ceramics co-doped with La^{3+} and Ca^{2+} ions. J Alloys Compd. 2014;586:136–41.
6. Li L, Fu R, Liao Q, Ji L. Doping behaviors of NiO and Nb_2O_5 in $BaTiO_3$ and dielectric properties of $BaTiO_3$-based X7R ceramics, Ceram. Int. 2012;38:1915–20.
7. Li L, Xie J, Wang M, Zhang K. Colossal permittivity (Nb, Mg) co-doped $BaTiO_3$ ceramics with excellent temperature stability and high insulation resistivity. Ceram Int. 2021;47:10072–8.
8. Wang X, Jia P, Sun L, Zhang B, Wang X, Hu Y, Shang J, Zhang Y. Improved dielectric properties in $CaCu_3Ti_4O_{12}$ ceramics modified by TiO_2. J Mater Sci: Mater Electron. 2017;29:2244–50.
9. Peng Z, Liang P, Chen X, Yang Z, Chao X. High thermal stability and excellent dielectric properties of a novel X8R - type $CdCu_3Ti_4O_{12}$ ceramics through a sol-gel technique. Mater Res Bull. 2018;98:340–8.
10. Hu W, Liu Y, Withers R, Frankcombe T, Noren L, Snashall A, Kitchin M, Smith P, Gong B, Chen H, Schiemer J, Brink F, Jennifer W. Electron-pinned defect-dipoles for high-performance colossal permittivity materials. Nat Mater. 2013;12:821–6.
11. Li L, Lu T, Zhang N, Li J, Cai Z. The effect of segregation structure on the colossal permittivity properties of $(La_{0.5}Nb_{0.5})_xTi_{1-x}O_2$ ceramics. J Mater Chem C. 2018;6:2283–94.
12. Peng H, Liang P, Zhou X, Peng Z, Xiang Y, Chao X, Yang Z. Good thermal stability, giant permittivity and low dielectric loss for X9R-type $(Ag_{1/4}Nb_{3/4})_{0.005}Ti_{0.995}O_2$ ceramics. J Am Ceram Soc. 2019;102:970–5.
13. Dong W, Hu W, Frankcombe T, Chen D, Zhou C, Fu Z, Cândido L, Hai G, Chen H, Li Y, Withers R, Liu Y. Colossal permittivity with ultralow dielectric loss in In + Ta co-doped rutile TiO_2. J Mater Chem A. 2017;5:5436–41.
14. Dong W, Chen D, Hu W, Frankcombe T, Chen H, Zhou C, Fu Z, Wei X, Xu Z, Liu Z, Li Y, Liu Y. Colossal permittivity behavior and its origin in rutile $(Mg_{1/3}Ta_{2/3})_xTi_{1-x}O_2$. Sci Rep. 2017;7:9950.
15. Wang X, Zhang B, Xu L, Wang X, Hu Y, Shen G, Sun L. Dielectric properties of Y and Nb co-doped TiO_2 ceramics. Sci Rep. 2017;7:8517.
16. Yang C, Tse M, Wei X, Hao J. Colossal permittivity of (Mg+Nb) co-doped TiO_2 ceramics with low dielectric loss. J Mater Chem C. 2017;5:5170–5.
17. Li J, Li F, Li C, Yang G, Xu Z, Zhang S. Evidences of grain boundary capacitance effect on the colossal dielectric permittivity in (Nb+In) co-doped TiO_2 ceramics. Sci Rep. 2015;5:8295.
18. Song Y, Liu P, Wu W, Zhou Q. High-performance colossal permittivity for textured (Al+Nb) co-doped TiO_2 ceramics sintered in nitrogen atmosphere. J Eur Ceram Soc. 2021;41:4146–52.
19. Liang P, Zhu J, Wu D, Peng H, Chao X, Yang Z. Good dielectric performance and broadband dielectric polarization in Ag, Nb co-doped TiO_2. J Am Ceram Soc. 2021;104:2702–10.

20. Dong W, Hu W, Berlie A, Lau K, Chen H, Withers R, Liu Y. Colossal dielectric behavior of Ga+Nb co-doped rutile TiO_2. ACS Appl Mater Interfaces. 2015;7:25321–5.
21. Zhao X, Liu P, Song Y, Zhang A, Chen X, Zhou J. Origin of colossal permittivity in $(In_{1/2}Nb_{1/2})TiO_2$ via broadband dielectric spectroscopy. Phys Chem Chem Phys. 2015;17:23132–9.
22. Wang X, Zhang B, Sun L, Qiao W, Hao Y, Hu Y, Wang X. Colossal dielectric properties in $(Ta_{0.5}Al_{0.5})_xTi_{1-x}O_2$ ceramics. J Alloys Compd. 2018;745:856–62.
23. Wang Z, Chen H, Nian W, Fan J, Li Y, Wang X, Ma X. Grain boundary effect on dielectric properties of $(Nd_{0.5}Nb_{0.5})_xTi_{1-x}O_2$ ceramicsceamics. J Alloys Compd. 2019;785:875–82.
24. Zhou X, Liang P, Zhu J, Peng Z, Chao X, Yang Z. Enhanced dielectric performance of $(Ag_{1/4}Nb_{3/4})_{0.01}Ti_{0.99}O_2$ ceramic prepared by a wet-chemistry method. Ceram Int. 2020;46:11921–5.
25. Peng H, Shang B, Wang X, Peng Z, Chao X, Liang P, Yang Z. Origin of giant permittivity in Ta, Al co-doped TiO_2: surface layer and internal barrier capacitance layer effects. Ceram Int. 2018;44:5768–73.
26. Li J, Yang S, Liu J, Zhuang Y, Tian Y, Hu Q, Xu Z, Wang L, Li F. Colossal dielectric behavior of Co-doped TiO_2 ceramics: A comparative study. J Alloys Compd. 2019;786:377–84.
27. Fan J, Leng S, Cao Z, He W, Gao Y, Liu J, Li G. Colossal permittivity of Sb and Ga co -doped rutile TiO_2 ceramics. Ceram Int. 2019;45:1001–10.
28. Li Z, Wu J, Xiao D, Zhu J, Wu W. Colossal permittivity in titanium dioxide ceramics modified by tantalum and trivalent elements. Acta Mater. 2016;103:243–51.

Figures

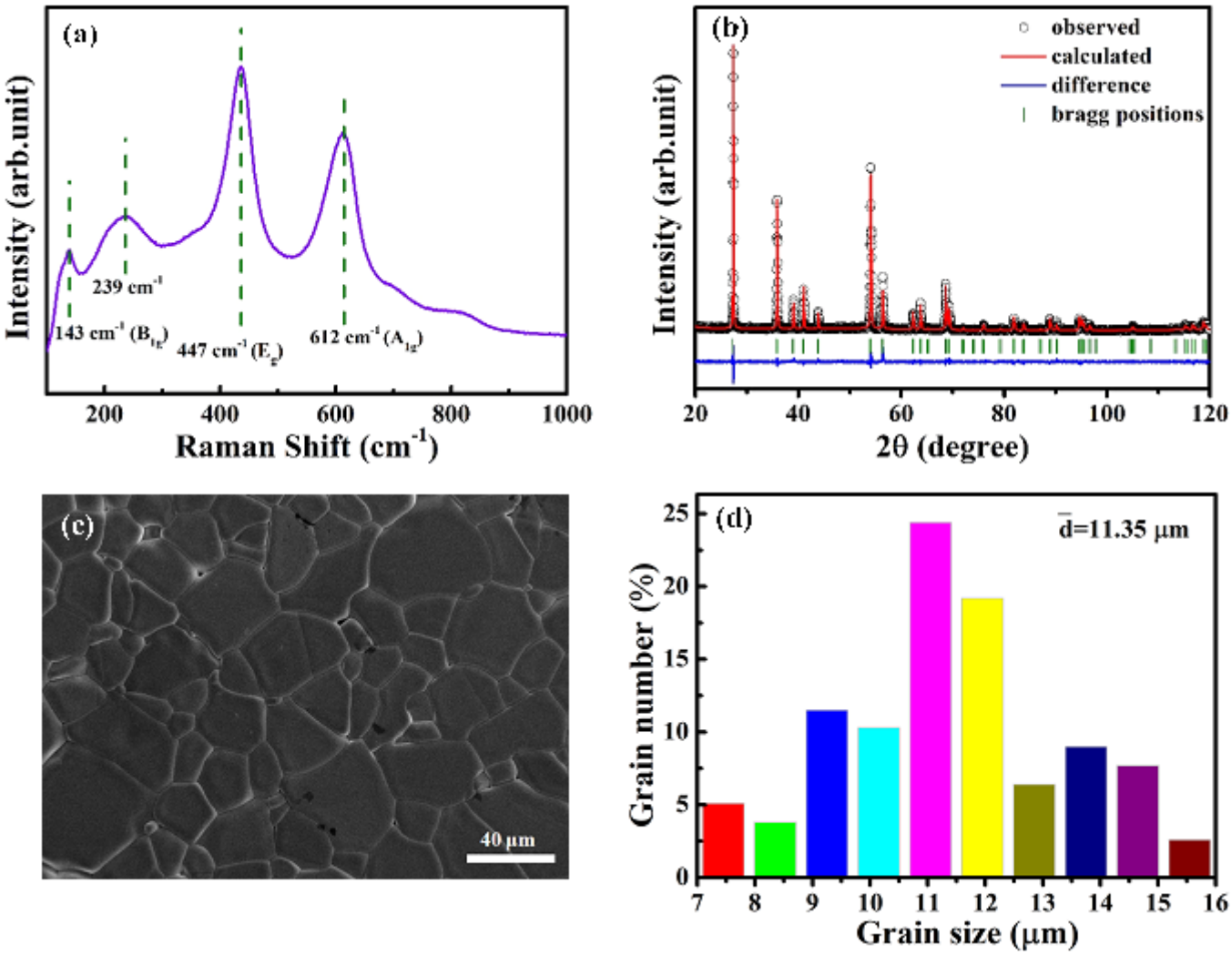

Figure 1

(a) Raman spectra, (b) Rietveld refinement fitting profile, (c) hot-corrosion surface SEM image, and (d) grain size of the ITTO ceramics.

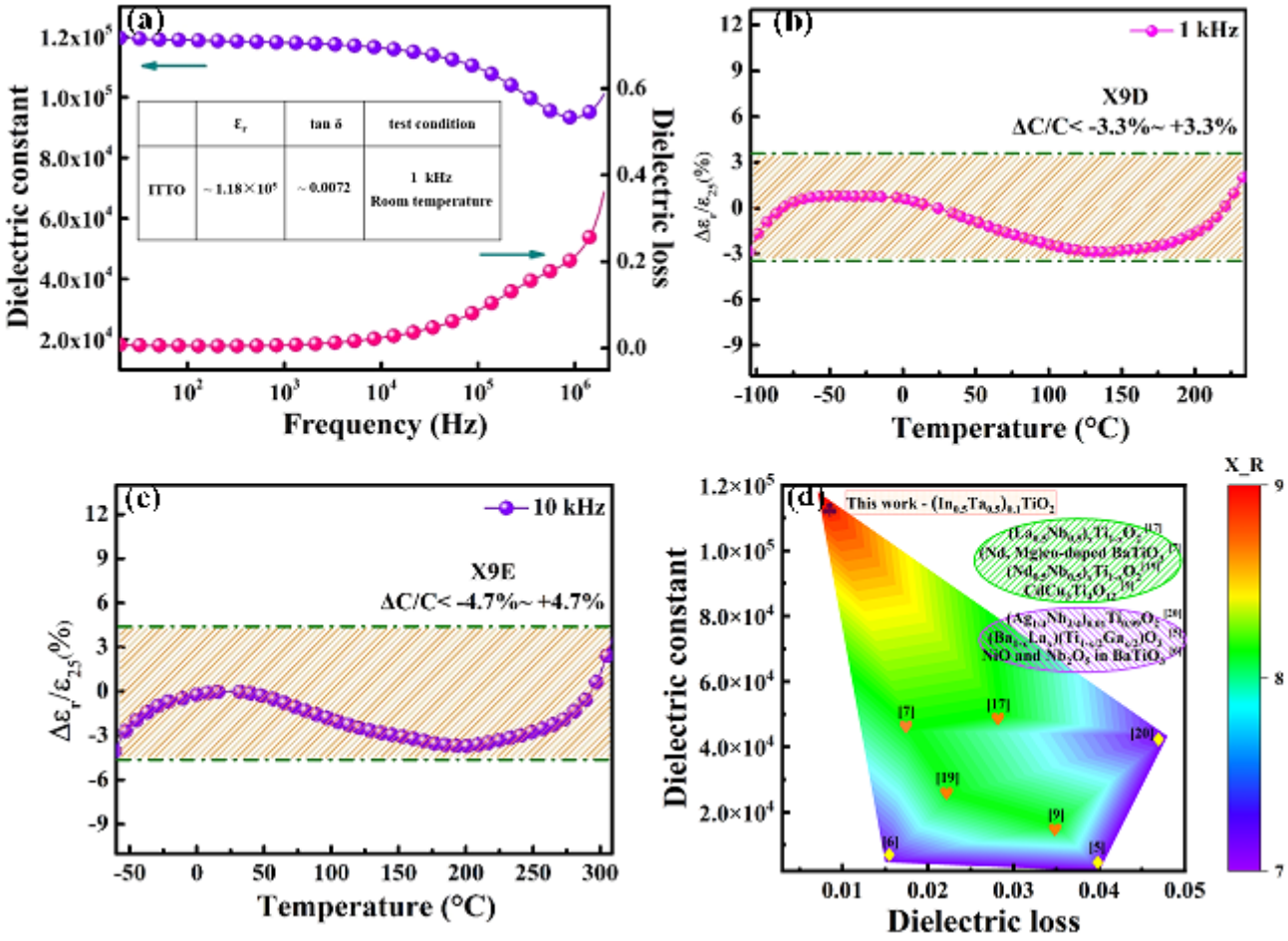

Figure 2

(a) Frequency dependent dielectric property of ITTO ceramics at room temperature. (b) Temperature coefficient of capacitance values of ITTO ceramics at 1 kHz, (c) 10 kHz. (d) Comparison of dielectric properties of the ITTO ceramics.

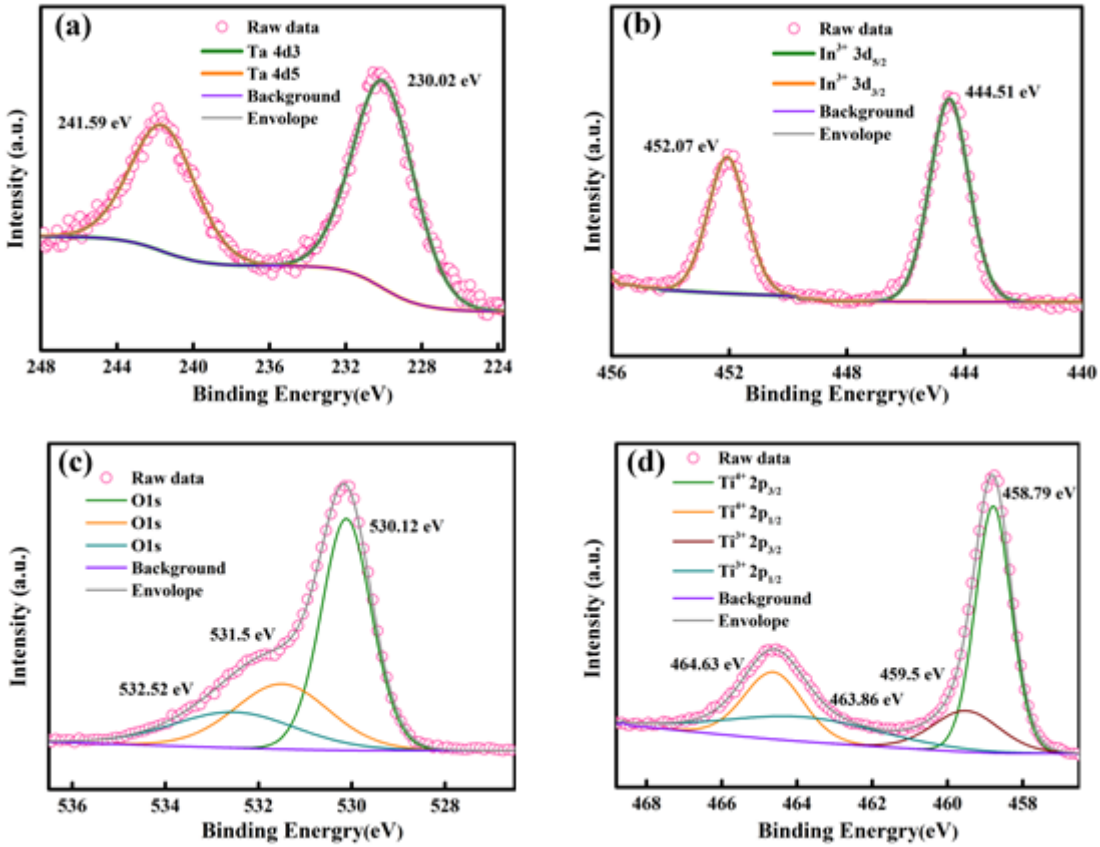

Figure 3

Valence state of various ions from XPS spectra and fitting data for the ITTO ceramics: (a) Ta 4d, (b) In 3d, (c) O 1s, and (d) Ti 2p.